

Elsevier required licence: © <2018>. This manuscript version is made available under the CC-BY-NC-ND 4.0 license <http://creativecommons.org/licenses/by-nc-nd/4.0/>  
The definitive publisher version is available online at <http://doi.org/10.1016/j.cplett.2018.06.018>

# Test of a polarized protein-specific force field in the molecular dynamics simulation of a protein crystal

Tingting Zhu,<sup>1</sup> Chao Wu,<sup>1</sup> Jianing Song,<sup>2</sup> Jeffrey R. Reimers<sup>1,3</sup>, Yongle Li,<sup>1\*</sup>

*1: Department of physics, International Center for Quantum and Molecular Structures, and Shanghai Key Laboratory of High Temperature Superconductors, Shanghai University, 99 Shangda Road, Shanghai 200444, China*

*2: NYU-ECNU Center for Computational Chemistry, NYU Shanghai, Shanghai, China*

*3: School of Mathematical and Physical Sciences, The University of Technology Sydney, Sydney NSW 2007, Australia*

**Keywords:** *protein crystal, MD simulations, polarized protein-specific charge*

Systematic molecular dynamics with different force fields are performed to simulate the structure and dynamics of a crystal of hen egg-white lysozyme, including AMBER and three versions of polarized protein-specific charge, PPC. The electrostatic polarization within the crystal is studied with a comparison among four resulting 250 ns trajectories. Results show that under appropriately parameterized PPCs, the protein can be stable during simulations, indicated by both smaller root-mean-square deviation and closer crystallographic B-factors to experimental values. This work also shows how the selection of dielectric constant affects the results of utilizing PPC.

---

\* Electronic address: [yongleli@shu.edu.cn](mailto:yongleli@shu.edu.cn)

## I. Introduction

X-ray crystallography is the preferred method to resolve the structure of proteins.[1] Although it needs protein crystals, which are different from the natural state, its ability to achieve very high resolution is indispensable. In the protein database, most resolved protein structures have been obtained using this method.

MD simulation is a powerful tool to reveal both the structure and dynamics of molecules in the condensed phase.[2-4] In recent years, MD has attained extraordinary success; with state-of-the-art super computer simulations of huge systems achieved within a few milliseconds. Recently MD simulation began to be applied to protein crystals.[5, 6]

Different from MD simulation in water, MD simulation of crystals leads application to highly inhomogeneous systems in which proteins are crowded together within a crystal lattice. Since the parameters of proteins are obtained from calculations which use proteins solvated in water, MD simulation of protein crystals remains challenging.[7] Only in recent years has there been some such successful MD simulations.[7-10] The force field parameters may not be perfect for simulating the crystallized phase as the results still deviate from experimental data. Previously, only a polarizable force field such as AMOEBA succeeded for the MD simulation of protein crystals.[11], but the time-consuming feature hindered widespread usage, partly due to the problem of combining polarizable or polarized parameters of protein with un-polarized parameters of water.[12] In a recent work, the polarized force field, known as the polarized protein-specific charge (PPC),[13] succeeded in predicting correct structures and dynamic behaviors in the solvated phase, yet suffered a similar deviation from experimental data.[9]

From published works, the non-negligible deviations from the experimental data include the distribution of water on the surface of proteins, and missing hydrogen bonds (H-bonds). From recent work, some major H-bonds within crystallized protein were destroyed during MD simulations, even with a polarized force field PPC in which the electrostatic polarization was considered to be good in liquid phase simulations.[9] It was proposed that the deviation stemmed from the inappropriacy of simulating non-electrostatic parts of the force field, such as van der Waals (vdW) effect, but without further validation. However, considering that vdW affects the system only in large space scale, while the backbone H-bond of the protein in a crystal is a local property that must be reflected by parameters related to electrostatic effects such as partial charge. So in this work, we systematically investigated the parameters generated by the PPC, by adjusting the major input parameter, the dielectric constant,  $\epsilon$ , which affects the property of the solvent simulated during quantum chemical calculations in preparing the PPC. We hope our investigation can help to reveal the effect of the electrostatic interaction in crystals, and help in the preparation of the PPC for the simulation of protein crystals.

The hen egg-white lysozyme (HEWL) is one of the most thoroughly investigated proteins,[14, 15]; one of its X-ray crystallographic structures is with an ultra-high resolution of 0.65 Å,[16]. Recently, L. Goerigk et al. investigated its crystal refinement by quantum chemistry,[17]. Such comprehensive structural information provided us with an ideal testing system. Thus, in this work, we have benchmarked MD simulation using

this highest resolution of HEWL crystal and evaluated the simulated polarization effect with different values of  $\epsilon$  used in the PPC.

## II. Methods

### a. Construction of the model system

The system is based on the experimental X-ray diffraction structure, with PDB entry 2VB1, and with space group P1 (shown in Figure 1). The cell constants are  $27.07 \times 31.25 \times 33.76 \text{ \AA}^3$ , and the three angles:  $87.98^\circ \times 108.00^\circ \times 112.11^\circ$ . There are four disulfide bonds between cysteine residues which stabilize the crystallographic asymmetric unit (ASU). In each unit cell, there is only one single-chain protein. Proteins between different cells are separated by unstructured water molecules, which cannot be recognized experimentally.

For preprocessing the protein structure we adopted the method proposed by Cerutti[6], so only a brief summary is provided here; further details can be found in previous works of MD simulations of protein crystals. From the downloaded experimental structure (entry 2VB1), we retained all the structural solvent molecules, including structural water, which are within 3  $\text{\AA}$  from protein, acetate acid anion (ACT), 1,2-ethanediol (EDO), and nitrate anion (NO3). For simplicity, we used the first position for each atom with multiple locations. Missing atoms were added by the tLeap module in the AMBER16 package, [18]. There were 1001 heavy protein atoms, 151 oxygen atoms belonging to water, 7 atoms in 1 ACT molecule, 30 atoms in 3 EDO molecules, and 36 atoms in 9 NO3 molecules.

To use periodic boundary conditions, (PBC) and reduce the error induced by the rigid lattice and symmetric long-range ordering, we constructed a super cell in a  $3 \times 3 \times 3$  arrangement to avoid the deficiency of using PBCs in our MD simulation. The central unit cell was created by the UnitCell module in the AMBER16 package. After constructing the super cell, we added extra water molecules by using another module, AddToBox, to simulate the condensation occurring experimentally.

For the protein, we used the popular AMBER99SB force field, [19], as a control group. For the PPC, we adopted the methodology in Mei et al.,[9] but used 3 different values of  $\epsilon$  for comparison: the default value  $\epsilon=80$  denoted as PPC1,  $\epsilon=10$  as PPC2, and  $\epsilon=20$  as PPC3. Thus the protein environment is considered with approximate  $\epsilon$  with value 10.  $\epsilon=20$  lies intermediate between the two extremes so may include the effect of water molecules in the crystal.

The force field parameters for solvent molecules other than water were taken from the generalized AMBER force field (GAFF), [20]; SPC/E, [21] was used for water. After optimization of the single cell, the PropPDB module in AMBER16 was used for constructing the super cell. The final model contained 52920 atoms belonging to 27 single-chain proteins, 27 ACT, 81 EDO and 243 NO3 molecules.

To obtain an appropriate number of water molecules, under each different force field we benchmarked several different numbers of water molecules, each with a 100 ns MD simulation. The optimum number was defined to be that which gave the lowest deviation in volume of the system compared with the experimental value. Then the systems with the optimum number of water molecules were used for production runs of 250 ns. Finally we obtained four 250 ns trajectories for further analysis, with the optimum number of water molecules as shown in Table 1.

### **b. Molecular dynamics simulations**

First we relaxed the entire model by 1000 steps of steepest-descent followed by another 1000 steps of conjugate gradient to minimize the water molecules while experimentally resolved protein atoms were fixed by a force constant of  $1000 \text{ kcal}\cdot\text{mol}^{-1}\cdot\text{\AA}^{-2}$ . The system was then heated to 800 K within 200 ps and kept at equilibrium for 10 ns to fully relax the water molecules. After this stage, the temperature was reduced to 292 K within 1 ns to mimic its growth temperature. Then we performed an 18 ns simulation at the same temperature with the restraint reduced stepwise from 1000 down to  $10 \text{ kcal}\cdot\text{mol}^{-1}\cdot\text{\AA}^{-2}$ , over 2 ns intervals for each step change in the value of the force constant: 1000, 800, 600, 400, 200, 100, 50, 20 and  $10 \text{ kcal}\cdot\text{mol}^{-1}\cdot\text{\AA}^{-2}$ . Throughout all these steps, the systems were maintained in NVT ensemble, and the periodic boundary conditions were applied. Then 100 ns production runs in NPT ensemble without any restraint were made on systems with different numbers of water molecules. After the optimum numbers of water molecules were determined for systems under different force fields, the production runs at 292 K were continued for 250 ns without restraint on them. All steps were performed with a 2 fs time step. The truncation of the van der Waals interaction was set to  $12 \text{ \AA}$ , and a particle meshed Ewald (PME), [22, 23] was used for long-range interactions. All other parameters were taken from standard protocols which may be readily found elsewhere, and were performed by the AMBER16 program package.

## **III. Results and discussion**

### **a. The overall structure of a protein crystal under MD simulations**

Since unstructured water is expelled from the crystal, but affects the structure and dynamics of protein within the lattice, we adopted the method provided by the AMBER program suit of adding water molecules used in the previous MD work. Water molecules were added and their effect assessed until the model system gave the volume deviation to within 0.3% relative error from the X-ray experimental data.

With this screening, we finally obtained the optimum number of water molecules, recorded in Table 1. All the trajectories are from 100 ns testing trajectories. The optima determined from AMBER and the other three versions of the PPC all lie within a relative error of around only 0.1%. The numbers are 6453 for AMBER, 6372 for PPC1, 6642 for PPC2, and 6615 for PPC3. It is of interest that the optimum numbers for AMBER and PPC1 are less than those for PPC2 and PPC3, and appears to indicate that the latter two can accommodate a greater number of water molecules. This observation can be explained by the difference in stability of the protein under different force fields. When AMBER and the traditional PPC1 are used, the backbone of protein becomes more flexible, so that the space remaining for water is reduced, so fewer water molecules are

able to remain in the crystal. The RMSD and B-factor analysis below further confirm this.

As introduced by Cerutti et al.,[6] there are two kinds of RMSD that can be obtained from the MD simulation of protein crystals: the crystallographic asymmetric unit (ASU) RMSD and the lattice RMSD. The ASU RMSD is defined as:

$$\text{ASU RMSD} = \sqrt{\frac{1}{M} \sum_{j=1}^M \left[ \frac{1}{N} \sum_{i=1}^N |\mathbf{r}_{i,j} - \mathbf{r}_{i,j}^*|^2 \right]} \quad (1)$$

Here  $M$  is the number of proteins within a single cell. Although in our case  $M$  is unity, the lattice RMSD curves still exceed their ASU RMSD counterparts, since they contain no rotational or translational imaging within the single lattice. The lattice RMSD may be used to investigate the effect of drifting of the center of mass of proteins within the single lattice. Both forms of RMSD curves are shown in Figure 2. The RMSD is the key feature of measurement describing the stability of the protein crystal under MD simulation. All ASU RMSD values are from the production run of 250 ns trajectories. The translational and rotational motion for each trajectory is removed before generating both kinds of RMSD. From the plot, the RMSD curves from the PPC are consistently below those from AMBER99SB. This feature of the PPC is well-known. However, the curve from the original PPC version, PPC1, is significantly above those from the PPC with less screening, PPC2 and PPC3. This contrast is reflected in the crystal phase, in which the number of water molecules is drastically limited compared to the liquid phase in which screening of water is significantly reduced. Every protein in a single cell is strongly affected by the surrounding proteins. So the original PPC overestimates the screening. One can also expect that the backbone of protein becomes more flexible under the original PPC with less electrostatic restriction from neighboring lattices. For the lattice RMSD, all the values become larger, since the drifting of the center of masses of proteins within the single cell is not removed. In lattice RMSD, one can see the RMSD curve from the AMBER increase gradually, suggesting that the structure will become deformed after longer MD simulation. All curves from the three versions of the PPC remain stable through time, and both curves from the two versions of the PPC with smaller  $\epsilon$  are very similar.

To measure further the stability of the structure, the B-factor should also be analyzed. This is an appropriate characteristic revealing the thermal motion of atoms around their mean positions, and may also be measured experimentally. In MD simulations, the B-factor of each atom can be obtained from the root-mean fluctuation from its trajectory:

$$B = \frac{8\pi^2}{3} F \quad (2)$$

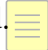
To investigate the stability of the protein crystal, the B-factor of all alpha carbon atoms was measured (shown in Figure 3). As RMSD has two forms, the B-factor also has the two forms. We calculated both forms of B-factor, as shown in both panels of Figure 3. In

our work, both B-factor plots appear similar, except for the regions with large B-factor values. Most positions of the backbone are observed to be highly conserved, excepting only five major regions, which reflect their high flexibility. Among these regions, four of them are pure coil and are intrinsically random. The major deviation segment, however, arises from the breaking of a backbone H-bond between V99@O and E102@N. This H-bond is well recognized from the experiment, but becomes broken during MD simulation under both AMBER and the traditional PPC. This break causes the turn region to become a random coil, leaving the B-factor to become exceptionally large. Once our scheme of the PPC is used, denoted as PPC3, the H-bond is mostly maintained, reflected by the B-factor of that region dropping drastically, nearly one-half of those from both AMBER and the traditional PPC.

#### **b. The backbone hydrogen bond (H-bond) related to the largest deviation of B-factor**

For a detailed analysis, we focused on the backbone H-bond formed by the residues which gave the largest deviation in B-factor. The structural information is recorded in Figure 4 and Table 2. Figure 4 shows the distribution of both bond length, defined by the two heavy atoms V99@O and E102@N, and the bond angle E102@N-E102@H-V99@O, from MD trajectories. The color scheme used is the same as that in the previous RMSD and B-factor analysis. Depth of color denotes the distribution of the snapshots with given angle, such that the darker the band, the more conformations there are with the value. The center of each data band is the mean value of the bond length, and the bandwidth denotes the standard deviation of the bond length. See Table 2 for the values. From the experimental structure, this backbone H-bond maintains a  $\beta$ -turn. From Figure 4, the distance given by the PPC3 is clearly closest to experiment, despite its value being stretched to  $3.96 \pm 0.14$  Å compared with the experimental value of 3.29 Å. This H-bond is broken for the trajectories from all the other three kinds of force field. For the AMBER trajectory, both the distance and angle distributions are large. The distance of the H-bond about the mean becomes  $4.19 \pm 0.21$  Å, and the angle is  $123 \pm 7.5^\circ$ . For the traditional PPC, this bond has similar length and the largest deviation,  $4.19 \pm 0.31$  Å, and angle  $127.4 \pm 6.8^\circ$ . Under both of these the H-bond is destroyed. For the PPC2 trajectory, in which an even smaller  $\epsilon$  is used during the charge fitting, the H-bond is destroyed even more decisively, which is evident as the distance increases to  $4.33 \pm 0.13$  Å, and the angle becomes the smallest,  $119.2 \pm 3.6^\circ$ . Both observations indicate a complete break in the H-bond, and consequently the loop region moves totally at random. In Figure 4, both PPC2 and PPC3 bands are observed to have smaller fluctuations in both distance and angle. This phenomenon is also likely to stem from the difference in screening of the crystal phase and of water, because the traditional PPC is fitted to the water environment, reflected by the  $\epsilon$  value used in simulating the solvation effect by the Poisson-Boltzmann equation [24, 25], whereas in the crystal environment the water/protein ratio is greatly reduced from near infinity to several hundred, (the number of water molecules in a single cell in this case is around 250). The failure of the PPC2 to give the correct H-bond may be caused by an overestimation of the electrostatic interaction, such that atoms with negative partial charges repel each other excessively.

To investigate further the stability of H-bonds from appropriately parameterized PPC during crystal phase MD simulations, we also calculated the total number of H-bonds

within the whole protein, including those in both backbone and side chains. The results in Table 1 show that the AMBER force field heavily underestimated, giving only  $54 \pm 1$  H-bonds. The traditional PPC gave even less with  $50 \pm 1$ , in contrast to its successes in the solution phase simulations. Again, this result reflects the traditional PPC overestimation of electrostatic screening within the crystal. Once  $\epsilon$  is reduced, the number of H-bonds immediately increases from around 50 to more than 70, much closer to the experimental value. Once again we see that a smaller  $\epsilon$  provides a better simulation of protein crystals. Conversely, although the number of H-bonds are the same from the two small  $\epsilon$  versions of the PPC schemes, the PPC with  $\epsilon=10$  failed to give the V99-E102 backbone H-bond. 

#### IV. Conclusions

In this work, we simulated a high-resolution crystal of protein, hen egg-white lysozyme (HEWL), using MD under the AMBER force field, traditional PPC and two refined PPCs. The inclusion of electrostatic polarization was observed to help stabilize the protein structure in the crystal phase. The selection of the value for the dielectric constant  $\epsilon$ , an important parameter, is also illustrated by a comparison of three different versions of the PPC. The MD with both AMBER and the traditional PPC can give almost the same RMSD curves, but the refined PPCs can give even lower and more stable RMSD curves. AMBER and the traditional PPC both failed to give good estimations of B-factors, but the refined PPCs worked well. This failure stems from giving an incorrect number of H-bonds, especially the H-bond contributing to maintain a beta-turn at the largest B-factor segment. All the results show that the PPC is still a successful method to simulate proteins in both solution and crystal phases, provided that the dielectric constant  $\epsilon$  is appropriately adjusted, although our work does not aim to provide optimal values for  $\epsilon$ . Such values may vary between systems, and a systematic methodology would be essential for their prediction. Otherwise, we recommend an effective estimation for  $\epsilon$ . For further enhancement of the performance of the PPC in MD simulations in the crystal phase, during the charge fitting stage explicit consideration would be needed of periodic conditions, such as Ewald summation.[26]

#### V. Acknowledgements

This study was funded by the National Nature Science Foundation of China (No. 21503130 to Y.L., No. 21603144 to J.S., and No. 11674212 to Y.L. and J.R.). Y.L. is also supported by the Young Eastern Scholar Program of the Shanghai Municipal Education Commission (QD2016021) and the Shanghai Key Laboratory of High Temperature Superconductors (No. 14DZ2260700). J.S. is also supported by the Shanghai Sailing Program (Grant no. 2016YF1408400). A part of the calculations has been done on the supercomputing system, Ziqiang 4000, in the High Performance Computing center in Shanghai University. Y.L. thanks Ye Mei, Mark Waller and Pavel Afone for their helpful discussions.



## Tables:

**Table 1:** Comparison of the optimum number of water molecules and number of H-bonds from MD simulations under different force fields. The experimental value is also shown. The different versions of the polarized protein-specific charge, PPC1-3, are explained in the text.

Method	$N_{\text{WAT}}^{\text{a}}$	$\epsilon^{\text{b}}$	$N_{\text{H-bond}}^{\text{c}}$
AMBER	6453	N/A	54±1
PPC1	6372	80	50±1
PPC2	6642	10	75±1
PPC3	6615	20	75±1
Expt.	N/A	N/A	79

a: Optimum number of water molecules giving smallest relative error of crystal volume to the experimental value.

b: Dielectric constant used for obtaining PPC.

c: Number of H-bonds during MD simulations.

**Table 2:** Comparison of backbone H-bond V99-E102 from MD simulations under different force fields and experiment. The different versions of the polarized protein-specific charge, PPC1-3, are explained in the text.

Method	Distance <sup>a</sup> /Å	Angle <sup>b</sup> /Degree
AMBER	4.19±0.21	123.0±7.5
PPC1	4.19±0.31	127.4±6.8
PPC2	4.33±0.13	119.2±3.6
PPC3	3.96±0.14	125.9±4.1
Expt. <sup>c</sup>	3.29	152

a: Distance between V99@O and E102@N.

b: Angle formed by the three atoms E102@N, E102@H and V99@O.

c: Measured from the crystal value from X-ray diffraction,[16].

## Figure Captions:

**Figure 1:** The overall structure of the crystal-phase protein HEWL in a single cell. PDB ID: 2VB1. The loop with the largest B-factor is shown in red.

**Figure 2:** Comparison of the RMSD of the backbone of protein from 250 ns MD simulations under different force fields. Both ASU and lattice forms are shown.

**Figure 3:** B-factor for alpha-carbon atoms from 250 ns trajectories of MD simulations under different force fields. The results of lattice B-factor are also compared with experimental values.[16] Both ASU and lattice forms are shown.

**Figure 4:** Comparison of the backbone H-bond between V99 and E102 related to the largest B-factor, obtained from MD trajectories under different force fields. The H-bond is defined as the distance between V99@O and E102@N, and the angle E102@N-E102@H-V99@O. Position and angle distributions are shown as bandwidth and depth of color.

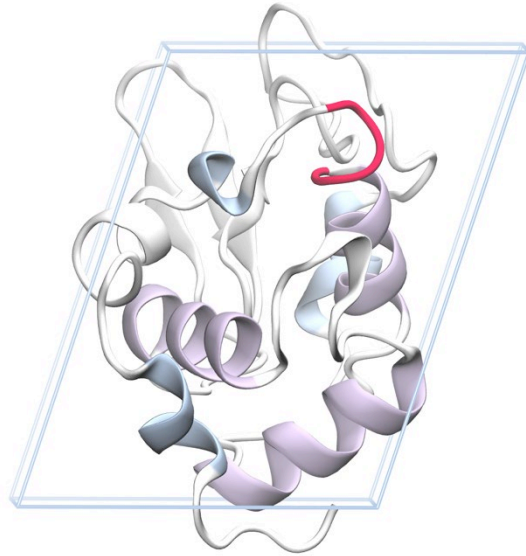


FIG 1: The single cell model of the HEWL crystal used in this work. The loop with the largest B-factor is shown in red.

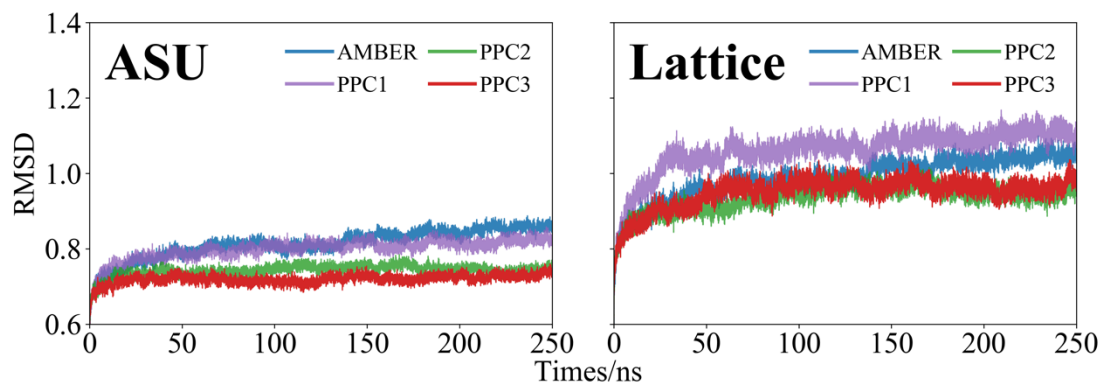


FIG 2: Comparison of RMSD from trajectories under different force fields.

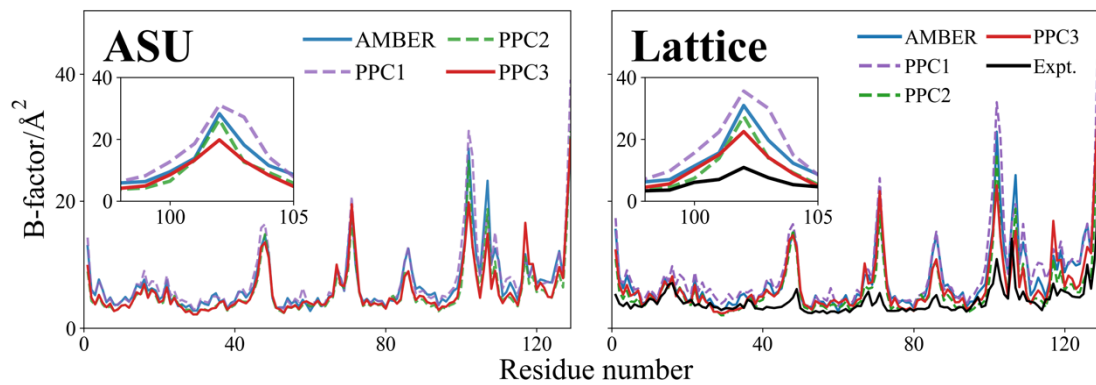


FIG 3: Comparison of B-factor from trajectories under different force fields. The experimental values are also shown.

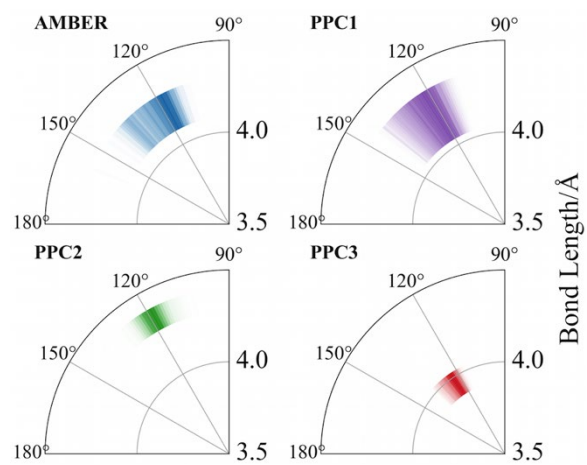


FIG 4: Comparison of the backbone H-bond between V99 and E102 from trajectories under different force fields.

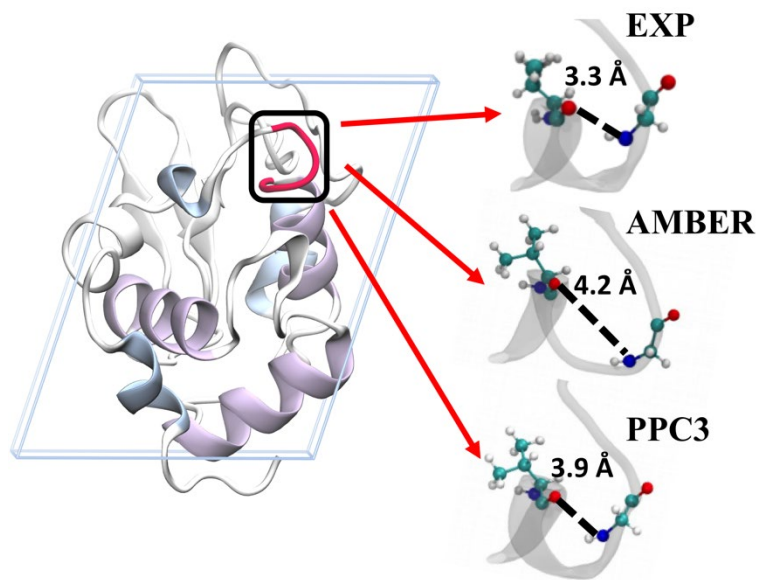


FIG 5: TOC: HEWL crystal and the hydrogen bond related to the largest B-factor, with the bond length given from different force fields; comparison with the experimental value.

- [1] Y. Shi, *Cell* **159** (2014), 995.
- [2] M. De Vivo, M. Masetti, G. Bottegoni, A. Cavalli, *Journal of Medicinal Chemistry* **59** (2016), 4035.
- [3] M.C. Childers, V. Daggett, *Molecular Systems Design & Engineering* **2** (2017), 9.
- [4] M. Bermudez, J. Mortier, C. Rakers, D. Sydow, G. Wolber, *Drug Discovery Today* **21** (2016), 1799.
- [5] D.S. Cerutti, I.L. Trong, R.E. Stenkamp, T.P. Lybrand, *Journal of Physical Chemistry B* **113** (2009), 6971.
- [6] D.S. Cerutti, P.L. Freddolino, R.E.D. Jr, D.A. Case, *Journal of Physical Chemistry B* **114** (2010), 12811.
- [7] P.A. Janowski, C. Liu, J. Deckman, D.A. Case, *Protein Sci* **25** (2016), 87.
- [8] P.A. Janowski, D.S. Cerutti, J. Holton, D.A. Case, *J Am Chem Soc* **135** (2013), 7938.
- [9] Y. Li, J.Z. Zhang, Y. Mei, *J Phys Chem B* **118** (2014), 12326.
- [10] J. Wang, *Bioenergetics: Open Access* **02** (2014).
- [11] J.W. Ponder, C. Wu, P. Ren, V.S. Pande, J.D. Chodera, M.J. Schnieders, I. Haque, D.L. Mobley, D.S. Lambrecht, R.A. DiStasio, M. Head-Gordon, G.N.I. Clark, M.E. Johnson, T. Head-Gordon, *The Journal of Physical Chemistry B* **114** (2010), 2549.
- [12] M. Betz, T. Wulsdorf, S.G. Krimmer, G. Klebe, *Journal of Chemical Information and Modeling* **56** (2016), 223.
- [13] C. Ji, Y. Mei, *Acc Chem Res* **47** (2014), 2795.
- [14] P.J. Artymiuk, C.C.F. Blake, D.E.P. Grace, S.J. Oatley, D.C. Phillips, M.J.E. Sternberg, *Nature* **280** (1979), 563.
- [15] J. Held, S. van Smaalen, *Acta Crystallographica Section D: Biological Crystallography* **70** (2014), 1136.
- [16] J. Wang, M. Dauter, R. Alkire, A. Joachimiak, Z. Dauter, *Acta Crystallogr D Biol Crystallogr* **63** (2007), 1254.
- [17] L. Goerigk, O. Falklöf, C.A. Collyer, J.R. Reimers, (2012), 87.
- [18] D.A. Case, T.A. Darden, T.E. Cheatham III, C.L. Simmerling, J. Wang, R.E. Duke, R. Luo, R.C. Walker, W. Zhang, K.M. Merz, B. Roberts, S. Hayik, A. Roitberg, G. Seabra, J. Swails, A.W. Götz, I. Kolossváry, K.F. Wong, F. Paesani, J. Vanicek, R.M. Wolf, J. Liu, X. Wu, S.R. Brozell, T. Steinbrecher, H. Gohlke, Q. Cai, X. Ye, J. Wang, M.-J. Hsieh, G. Cui, D.R. Roe, D.H. Mathews, M.G. Seetin, R. Salomon-Ferrer, C. Sagui, V. Babin, T. Luchko, S. Gusarov, A. Kovalenko, P.A. Kollman, AMBER 16. University of California, San Francisco, San Francisco, 2016.
- [19] H. Viktor, A. Robert, O. Asim, S. Bentley, R. Adrian, S. Carlos, *Proteins: Structure, Function, and Bioinformatics* **65** (2006), 712.
- [20] W. Junmei, W.R. M., C.J. W., K.P. A., C.D. A., *Journal of Computational Chemistry* **25** (2004), 1157.
- [21] H.J.C. Berendsen, J.R. Grigera, T.P. Straatsma, *The Journal of Physical Chemistry* **91** (1987), 6269.
- [22] T. Darden, D. York, L. Pedersen, *The Journal of Chemical Physics* **98** (1993), 10089.
- [23] U. Essmann, L. Perera, M.L. Berkowitz, T. Darden, H. Lee, L.G. Pedersen, *The Journal of Chemical Physics* **103** (1995), 8577.
- [24] G.M. K., H. Barry, *Proteins: Structure, Function, and Bioinformatics* **4** (1988), 7.



[25] B. Honig, A. Nicholls, *Science* **268** (1995), 1144.

[26] Y. Zhou, S. Wang, Y. Li, Y. Zhang, in: A.V. Gregory (Ed.), *Methods in Enzymology*, Academic Press, 2016, p. 105.